A ROTATING PLASMA AS A SOURCE FOR INJECTION INTO A MAGNETIC MIRROR

By

H. K. Forsen and A. W. Trivelpiece

ERL Technical Memorandum M-145
18 January 1966

ELECTRONICS RESEARCH LABORATORY
College of Engineering
University of California, Berkeley
94720

This work was supported primarily by National Science Foundation Grant GP-2239 and in part by Air Force Avionics Laboratory Contract AF-33(615)-1078. This paper is based partially on a thesis submitted in June 1965, by one of the authors (H. K. F.) to the University of California, Berkeley, in partial fulfillment of the requirements for the Ph.D. degree.

ABSTRACT

A two-stage, magnetic-mirror, compression experiment was constructed to investigate a rotating plasma as a clean, high-temperature, plasma source. Kilovolt deuterons are created in the static, crossed-electric, and magnetic fields of the first stage for transfer or injection into the second stage. It was found that the purity of the plasma is limited by electrode effects and that anomalous plasma loss occurs along the flux lines through the mirrors. These electrode effects are described and explained. The plasma loss is related to an instability associated with the anisotropic velocity distribution.

I. INTRODUCTION

Ionization in static, crossed electric and magnetic fields results in a drift motion for both ions and electrons that is perpendicular to both $\vec{E}$ and $\vec{B}$ at a speed $v_D = E/B$. Circular motion is superposed on this drift motion at the gyrofrequency. There is equal energy in the drift motion and in the gyromotion (i.e., $W_D = W_G = \frac{1}{2} m v_D^2$). Since the drift velocity is not a function of the charge or mass of the particle, the kinetic energy is proportional to the mass and the ions have considerably more energy than the electrons.

A number of experiments conducted to study rotating plasmas in radial-electric and axial-magnetic fields have been reviewed by Wilcox[1] and more recently by Tozer.[2] The recent ideas of Halback and Baker[3] about the "Puffatron" device have promoted new interest in rotating plasma devices as means of creating a hot-iron plasma. The Puffatron approach has the advantage of a low base pressure vacuum system into which a limited amount of neutral gas, as necessary for ionization and plasma formation, is injected.

This paper reports on experiments designed to use a puffatron-type rotating plasma as a source for a two-stage, magnetic-mirror compression experiment.[4] The plasma is created in the first stage by injecting deuterium gas from a plenum within the center electrode into a radial-electric and axial-magnetic field configuration. The gas is ionized by avalanche breakdown. This rotating plasma is then transferred to the second stage, out of the region of the central anode, for additional adiabatic compression. Two methods of plasma transfer were studied.

One involved the use of a traveling magnetic-mirror field; the other involved the use of a gradient magnetic field to accelerate the plasma out of the first stage. The problems of creating, confining, and transferring a rotating plasma, and the problems introduced by the metallic electrodes, are discussed.

II. EXPERIMENT

A. Description

The two-stage, magnetic-mirror compression experiment used in this study is shown schematically in Fig. 1. The first stage, where the plasma is created, is shown in the upper half of the figure. The second stage, where the plasma transfer and trapping are studied, is directly below the first stage; the vacuum system and longitudinal access port are directly below the second stage. The vacuum chamber is a stainless steel tube, 10 cm diameter, 0.7 mm thick, and with a magnetic diffusion time constant of about 35μsec. The trapping, transfer, and compression coils are outside of the vacuum chamber. Several radial diagnostic ports are provided by stainless steel tubes (1.27 cm diameter) that extend from the liner out through the magnetic coils in both the first- and second-stage sections.

At the upper end of the vacuum chamber a ceramic section is both the support and the electrical insulator for the coaxial conductor and puff-valve actuator system. The stainless steel center conductor (2.54 cm diameter) extends through the first stage and is the anode for the radial electric field. This center conductor is hollow and is used to admit the charge of neutral gas into the vacuum chamber through the several small ports around the center conductor and midway between the first and third magnet coils. The gas puff valve is located next to the gas injection ports and is actuated by an elastic wave that propagates down a stainless steel rod inside the hollow center conductor. The end of this stainless steel rod is ground to form a "knife edge" that is

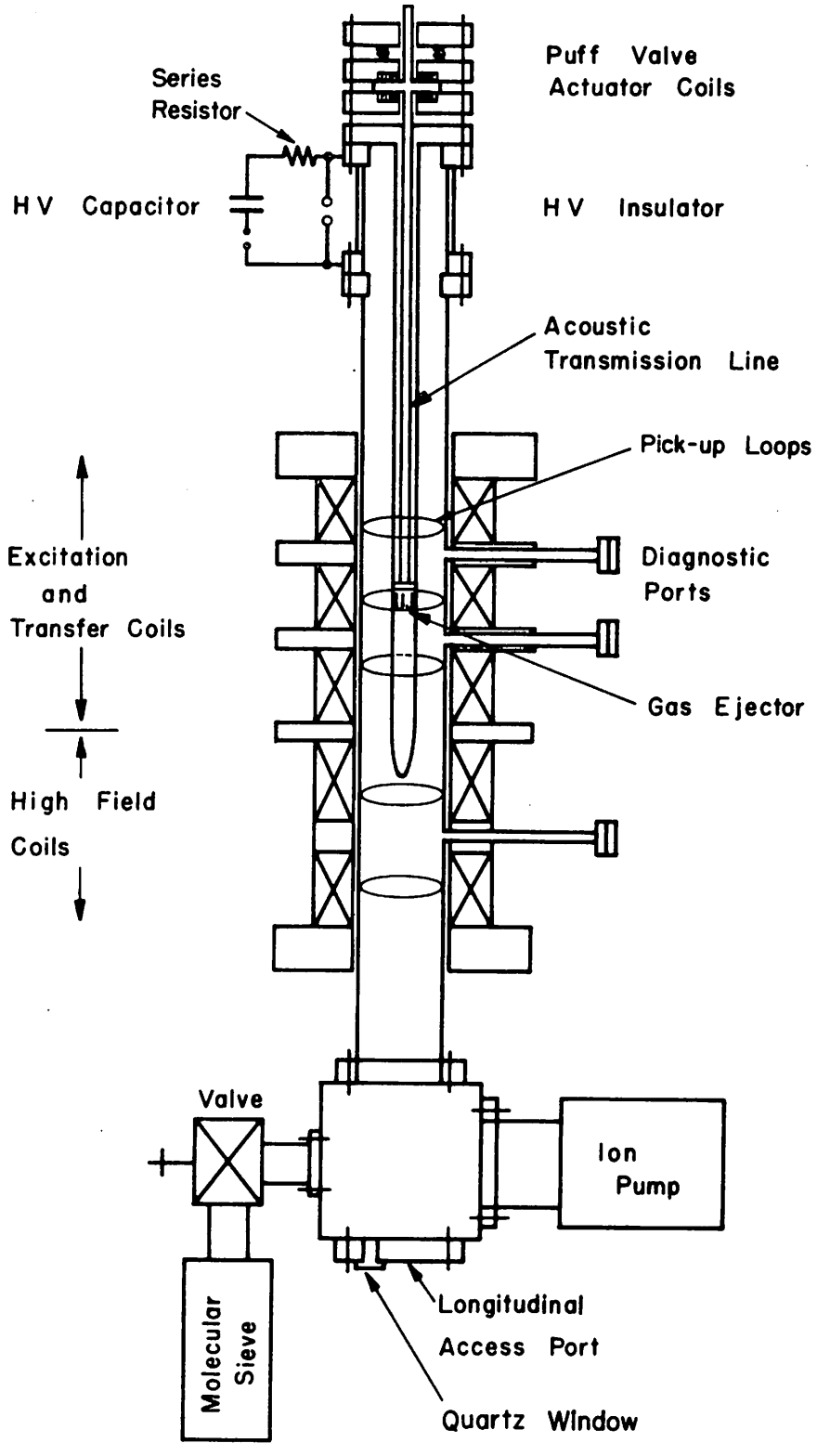

Fig. 1. Schematic diagram of the two-stage experiment.

pressed into a soft seat (nylon or copper).[5] When the elastic wave reflects from the end of the rod, the knife edge lifts from the valve seat. This discharges the predetermined gas load from the plenum. At the upper end of the stainless steel rod, the elastic wave is launched by means of a pulsed coil that delivers a mechanical impulse to a disk attached to the rod.

The base pressure of the all-metal system is approximately 2×10^{-8} torr, but most experiments were performed at 4 to 6×10^{-7} torr. The radial electric field between the central anode and the outer cathode is provided by means of a fast capacitor (2.0 μfarad, 50 kV) that electrically connects anode and cathode through a spark-gap switch. A series 1.2 ohm resistor limits the current in the event of internal shorting. A second spark-gap switch connected across the cathode-anode circuit at the high-voltage insulator turns off the electric field after initial avalanche breakdown.

Energy for the pulsed magnet coil system is provided by a sectionable, programmed, 0.25-megajoule capacitor, energy-storage bank. The nominal first-stage magnetic field is 18 kG at the center and can be changed in 30μsec to transfer the plasma to the second stage. The capacitor bank can provide a field of 60 kG (mirror ratio 1.5:1) in the second stage.

B. Operation

The normal sequence of operation of the experiment starts with the launching of an elastic wave down the valve-actuating rod. This opens the valve and discharges 10^{17} D_2 molecules from the anode plenum into the cathode-anode region. The nominal, axial-magnetic field in

this region is 18 kG; the nominal, cathode-anode voltage is 25 kV. Ionization avalanche occurs about 60μsec after the puff valve opens. The typical, resultant voltage and current waveforms are shown in Fig. 2. In addition to the expected avalanche breakdown, a second breakdown results in an internal cathode-anode short circuit which rapidly reduces the electric field to zero. This internal crowbarring is an electrode effect and is discussed in a later section.

From the conservation of angular momentum, it is possible to estimate the density of a rotating plasma:

$$r\ nm\ v_D \hat{k} = \int_0^{\tau} \vec{J} \times \vec{B} \times \vec{r}\ dt, \tag{1}$$

where $\hat{k}$ is a unit vector in the z-direction. The integrand is independent of time except for $\vec{J}$, therefore the impulse torque is a result of the initial avalanche current. The drift speed is $v_D = E/B$, and the total charge transferred is $Q = \int I dt$. For an azimuthally symmetric plasma shell of length L at radius r, the electric-field, particle-density product is

$$nE = \frac{QB^2}{2\pi r L m}. \tag{2}$$

If the electric field is known, it is possible to determine the density. The dependence of this equation on magnetic field was confirmed by repeating the experiment at different magnetic fields for a fixed electric field and a quantity of injected gas. Figure 3 shows that I or Q (avalanche period is constant) varies as B^{-2}. This implies that the density is constant even for a large particle gyroradius.

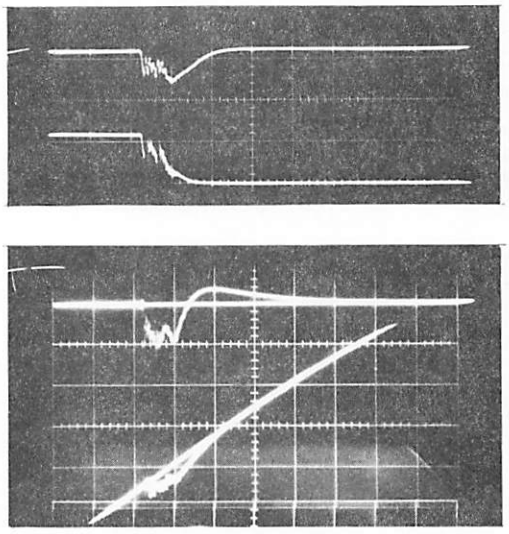

Fig. 2. Current, voltage, diamagnetic loop, and B_Z prove waveforms. 10 μs/cm.

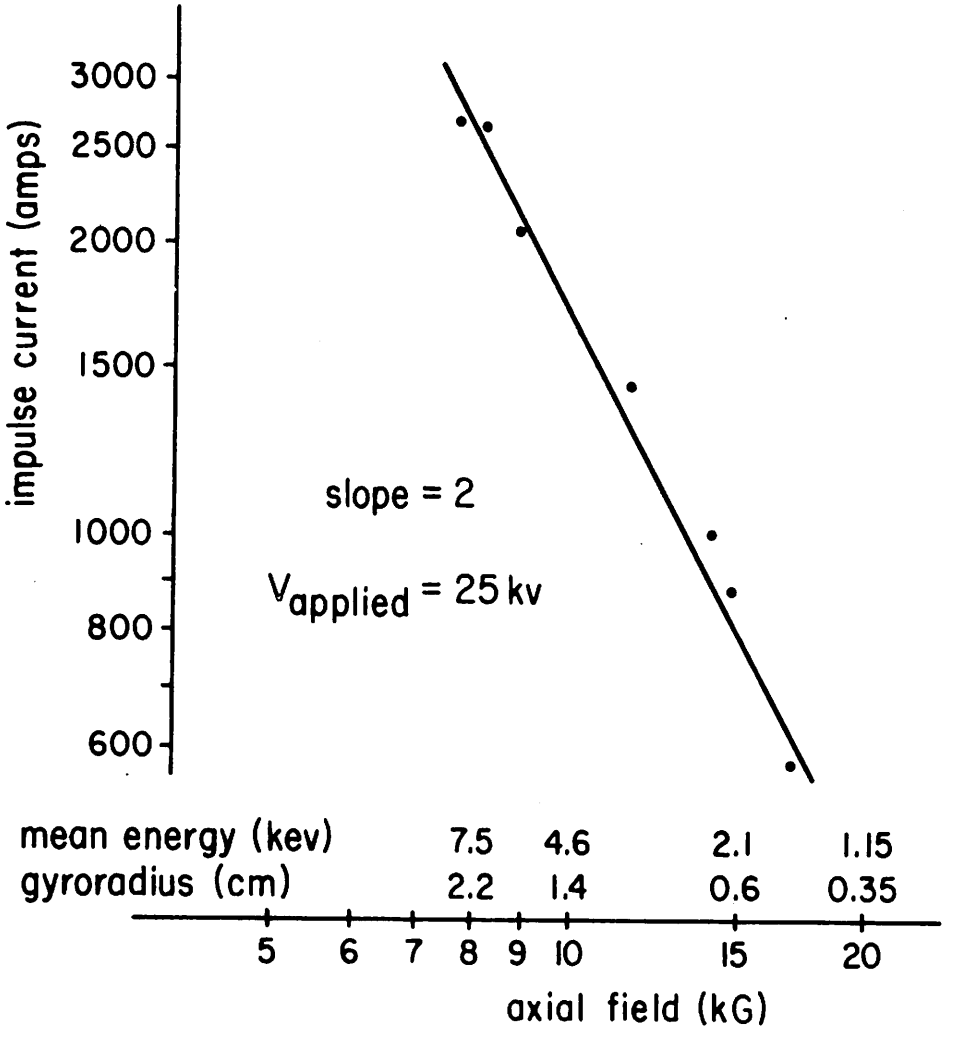

Fig. 3. Plot of the variation of the avalanche current vs the applied magnetic field. The quantity of injected gas and the applied voltage are constant.

The density can also be checked by the equivalent hydromagnetic capacity.[6] To obtain an expression for this capacity, Eq. 1 is integrated with respect to radius, and it is assumed that the particle density is independent of radius. The experimental value of 0.3 μfarad for the hydromagnetic capacity is obtained from the peak voltage (Fig. 2) following the avalanche breakdown, the driving capacitor (2.0μ farad), and the circuit capacitance. The total dielectric constant, $\kappa_e = (1 + nm/\epsilon_0 B^2)$, for the experiment is 7×10^4 which corresponds to a density of 2×10^{14} cm^{-3} for this case where the magnetic field was 11.0 kG. If the electric field is constant across the electrode region, an average density of 2×10^{14} cm^{-3} is also obtained from Eq. 2. Justification for the assumption of a constant electric field is based on a theoretical calculation.[7] However, there is no direct experimental measurement to confirm this point because insertion of a probe would eliminate the rotating plasma. Measurements made on the Ixion[8] experiment indicate a 1/r or faster decrease of electric field with radius. However, the Ixion result does not apply here since the slower ionization rate for that experiment is not consistent with the assumption used to obtain Eq. 2.

To calculate the drift velocity or the density, it is first necessary to obtain an estimate of the electric field which depends on the electrode separation. For this experiment there is an effective electrode separation that is less than the cathode-to-anode distance. This reduced separation is a result of the fact that the mirror magnetic field lines, which are curved from the anode into the cathode-anode region, are

equipotentials as a result of the high electron density. The vacuum flux surface in Fig. 4 illustrates this point. For a mirror ratio of 1.5:1, the distance between the extreme flux surface that is at the anode potential and the cathode is 3.44 cm. For this effective separation the electric field at an applied voltage of 25 kV is 7.3×10^3 V/cm. If there are no large sheath effects,[9] this electric field corresponds to a drift speed of 4×10^7 cm/sec.

To measure the energy density of the plasma, its diamagnetic flux was measured by pick-up loops (Fig. 1) and magnetic probes inserted just inside the vacuum chamber through the radial ports. The loops measure the total flux drop; the probes measure the magnetic field increase. When the corrections are made for the metal vacuum chamber, both methods predict an energy density of about 0.1 joules/cm^3. This value is consistent with a density of 2×10^{14}/cm^3 and an ion temperature of 1670 eV, providing there is an equal energy in gyromotion and in bulk rotation. Figure 5 shows a typical signal from a diamagnetic loop (ΔB) and from the magnetic probe (B_z) for a case where the plasma is lost in about 15-30μ sec after initial avalanche.

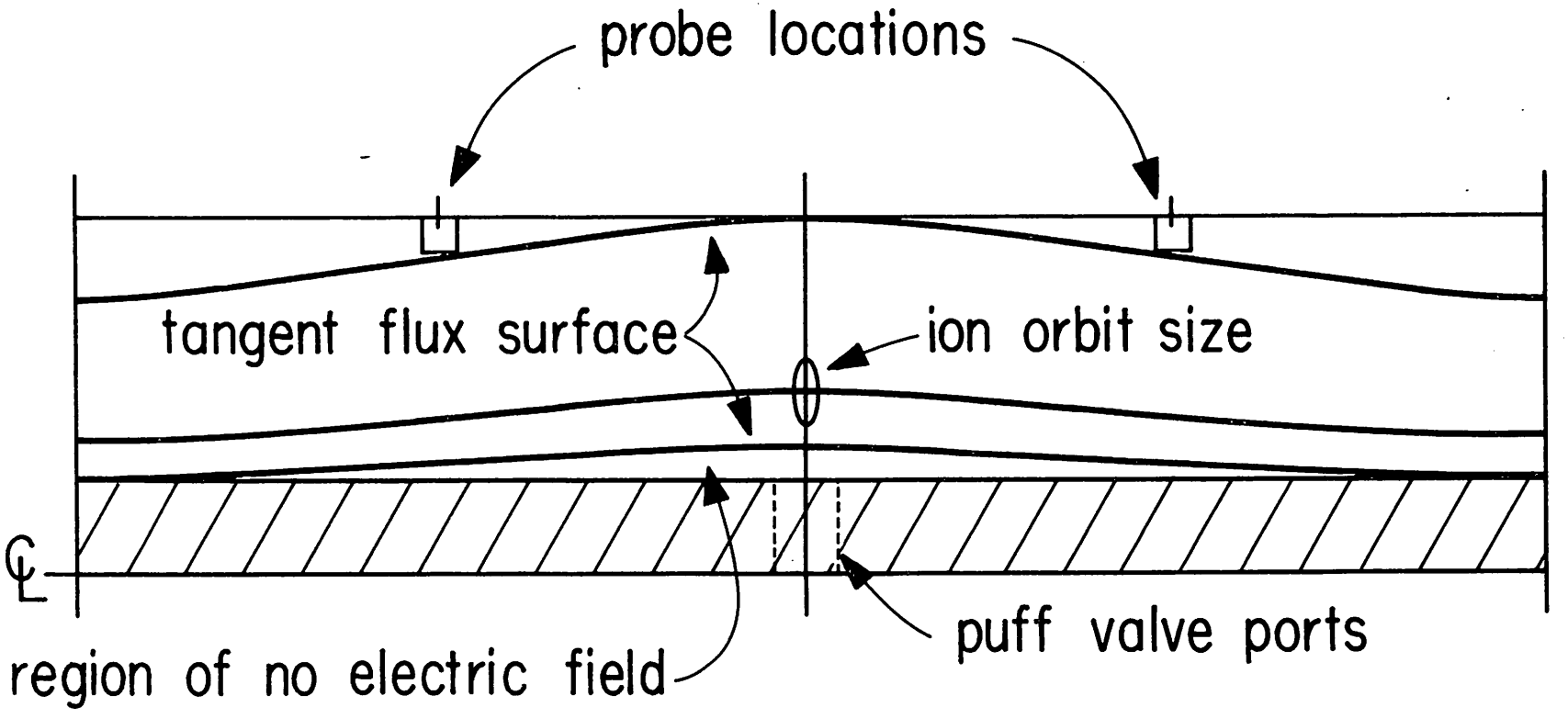

Fig. 4. Typical vacuum flux surfaces, ion orbit, and probe locations.

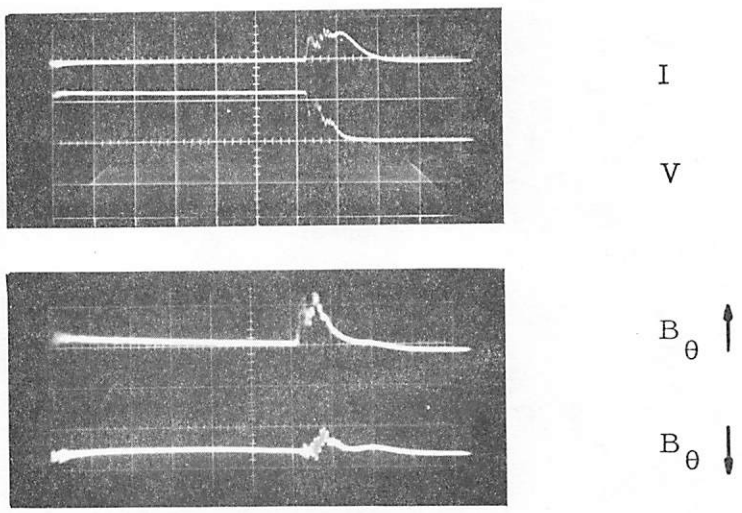

Fig. 5. Current, voltage, upper and lower B_θ waveforms. 10 μs/cm.

III. RESULTS AND DISCUSSION

A. Internal Crowbar

Several processes cause breakdown or internal short circuit within the cathode-anode region. The simplest is a result of the fringing electric and magnetic fields outside of the first-stage mirror region. Fringing magnetic field links the center electrode with the outer electrode, but fringing does not occur at both ends of the first stage because flux lines from the first stage map into the second stage whenever the second-stage field coils are energized. Fringing electric field occurs because the anode does not extend much beyond the lower mirror peak of the first stage. These fringing fields result in a situation where $\vec{E} \cdot \vec{B} \neq 0$, a condition that usually leads to a low impedance short if either neutral gas or plasma enters such a region. The short discharges the driving capacitor and reduces the electric field to zero, which in turn results in a polarization drift of ions back into the anode. The shift of the ion guiding center back to the potential surface from which it was born (about a gyroradius) results in that portion of the plasma within a gyroradius of the anode striking it. This liberates enough surface gas to destroy the plasma.

To illustrate this polarization effect, note that a charged particle born in static, crossed electric and magnetic fields moves in the direction of the electric field so that its guiding center shift exactly accounts for the energy in gyromotion and drift motion. If the electric field is adiabatically reduced to zero, the drift motion is lost and the guiding center moves back to the location of the equipotential

from which it started and the gyromotion is unchanged. This is illustrated by a calculation of the change in radius of the guiding center, as the electric field is removed. The integral of the polarization drift is

$$r = \int_0^{\infty} v_p \, dt = \frac{m}{eB^2} \int_{E_0}^{0} dE = -r_G, \tag{3}$$

where

$\vec{v}_p = \frac{m}{eB^2} \frac{d\vec{E}}{dt}$ and r_G is the gyroradius.

The corresponding energy removal is

$$\mathcal{E}_r = \int_0^{r_G} E(t) dr = e \int_0^{\infty} E(t) \frac{dr}{dt} dt. \tag{4}$$

For an exponential decay of electric field with time and $dr/dt = v_p$, Eq. 9 reduces to

$$\mathcal{E}_r = (1/2) m v_D^2. \tag{5}$$

This result is valid for a uniform magnetic field. It must be modified for the case of a spatially varying field such as in the experiment discussed here. A more exact calculation does not substantially change the results.

Evidence that such an effect occurs is demonstrated by the observed erosion of the anode between the regions of the mirror peaks. This region is less than the distance between the mirrors by the projected gyroradius from the last tangent flux surface of Fig. 4.

Electrons which strike the anode do not have enough energy to cause the observed erosion.

A reduction of the $\vec{E} \cdot \vec{B} \neq 0$ internal crowbar, is obtained by energizing the second-stage magnetic field. This maps the flux lines down the device some 40 cm before the fringing field of the lower second-stage mirror allows lines from the anode to connect with the cathode. Another method would be to extend a reduced diameter anode through both stages of the device. For most cases, experimental operation under conditions of extended flux surfaces did not result in breakdown at the anode tip. There still remained a slower breakdown at the fringing field above the upper mirror, however, this could be minimized by insuring that the electric field was on before the influx of gas from the puff valve. This operating condition reduced the number of neutrals to reach the fringing field region.

There is a more complicated internal crowbar mechanism that is a result of the properties of the plasma itself. If the ratio of particle pressure to magnetic pressure is large $\beta > 0.1$, or if the field configuration is that of a magnetic mirror, there is a symmetric axial gradient of magnetic field. This means that in the plasma region, the flux surfaces are not parallel to the anode but are bowed as shown in Fig. 4. These magnetic flux surfaces are equipotentials, and the entire region between the last flux surface tangent to the anode (tangent surface in Fig. 4) and the anode is filled with cold plasma at the anode potential. In addition, an up-stream internal short also reduces the electric field after avalanche and results in a polarization drift of some ions back to

the anode. Both of these processes liberate neutral impurity atoms from the anode. These neutrals then become ionized and scatter into the region where there is an electric field. These impurities have a larger mass-to-charge ratio than the deuterons. Therefore, they have a gyroradius that is too large to be contained and quickly go to the outer cathode. These high-mass impurity ions that go to the outer cathode result in an ion current which drains energy from the driving capacitor and further reduces the electric field. This results in additional polarization drift of deuterons into the anode. Consequently, more impurities are liberated and a cumulative process continues until the driving capacitor is discharged.

The upstream internal short makes it difficult to separate these two processes. Internal breakdown along flux lines is difficult to reduce. However, the evidence of its occurrence is clear. Outside of the mirror field, where the anode and the cathode are linked, surface erosion on the anode is very pronounced. The liberated ionized impurities follow flux lines to the cathode and deposit observable quantities of stainless steel along the inside surface of the Al_2O_3 insulator. Although the quantity of impurities liberated between the mirrors by the polarization drift is small by comparison, their current is measurable by the difference signal obtained from magnetic probes inserted just inside the cathode (see Fig. 4). When these probes are rotated to measure the B_θ field produced by the J_z current down the center electrode, they produce the waveform shown in Fig. 5. By comparing the initial avalanche current with the initial current as measured by the upper B_θ probe, comparable results are obtained.

This indicates that the avalanche current flow is measured by the current transformer and the upper B_θ probe, but not the lower B_θ probe. This means that the avalanche current passed between the two probes and therefore through the bulk of the plasma, as would be expected. Subsequently, the current associated with the upstream crowbar is determined from the difference signal between the upper probe and the current waveform. The small tip current is measured by the lower probe, and the late current that passes between the two B_θ probes is measured by the difference in the two probe signals. This current, which is not zero, is accounted for by the proposed model of impurity shorting.

B. External Crowbar

The electric field can also be removed externally by the spark-gap switch connected between the cathode and anode outside the vacuum system. If this external crowbar switch is triggered just after the initial avalanche breakdown, internal crowbar does not occur. Rapid removal of the electric field (in less than a gyroperiod) results in conversion drift energy into gyroenergy, as in the Moscow Ion Magnetron.[10] However, slow removal of the electric field (over many gyroperiods) has the deleterious effect of causing the polarization drift of ions into the anode such that all particles within a gyroradius of the anode, or the tangent surface of Fig. 4, strike the anode and liberate impurities. Since the plasma density varies as 1/r, from Eq. 2, this represents a sizeable loss of magnetic fields below 30 kG. In addition, the "self-cleaning" feature of a rotating plasma, which tends to trap

impurity ions on the cathode, is lost when the electric field is removed.

Figure 6 shows the difference in the current and voltage waveforms and the corresponding bremsstrahlung and D_β radiation for the cases where the discharge is (a) internally crowbarred and (b) externally crowbarred. The larger bremsstrahlung flux for external crowbar is not thought to be due to radiation from electrons, but is more likely due to gamma radiation from energetic ions that drift back into the anode as a result of depolarization effects. In Fig. 6a it is shown that the radiation starts to decrease after avalanche breakdown. This occurs during the period of constant electric field prior to internal crowbar. The radiation then increases as the electric field decays. As shown in Fig. 6b, the effect is more pronounced when the experiment is crowbarred externally. The detector was shielded from radiation from the upstream internal crowbar and was situated so as to receive radiation at a radial diagnostic port whose line-of-sight axis intercepted the anode. Oscillations occurring on the current and voltage waveform have a radian frequency of about 1.6×10^7, i.e., the frequency at which an ion travels around the mean radius of the chamber. This may mean that the breakdown is not axissymmetric, but it was not confirmed by photographs of the discharge through the longitudinal port. Such photographs showed a hot plasma between the electrodes and a halo of light around the cathode, which was expected from impurity recombination in that area.

Diamagnetic signals indicate that the plasma is lost from the first-stage mirror region at about the same rate as the electric field

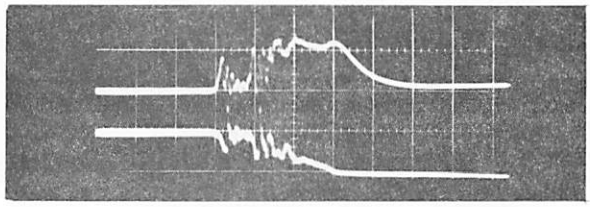

I

V

(a)

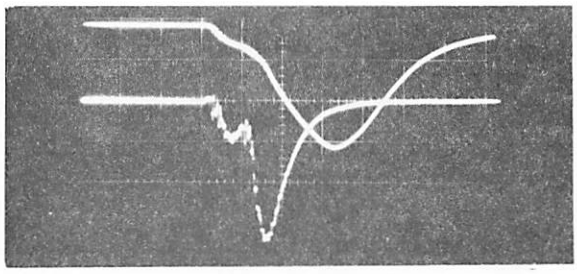

D_β

Bremsstrahlung

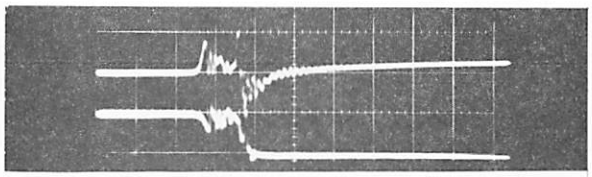

I

V

(b)

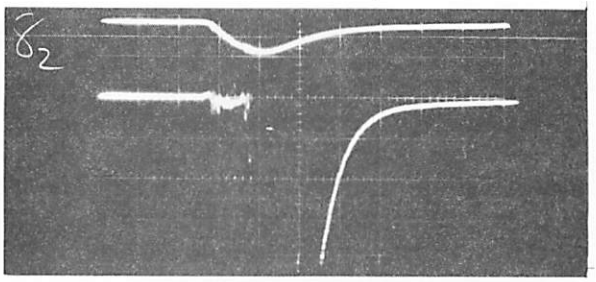

D_β

Bremsstrahlung

Fig. 6. Current, voltage, D_β, and bremsstrahlung radiation for internally (a) and externally (b) crowbarred discharges. 5 μs/cm.

decay (see Fig. 2). This is about 15-30μsec, for internal crowbar and less than 5μsec on external crowbar. This rapid loss cannot be explained solely from impurity influx.

C. Plasma Loss

In addition to the loss of plasma to the anode by polarization effects, there is also axial loss of plasma from the first stage. This loss of plasma is independent of the first-stage magnetic field configuration. There is no basis for relating this loss of plasma to any particular mode of instability; however, the anisotropic velocity distribution function is the most likely class of instability.

To measure the loss of ions along the magnetic field lines through the second-stage mirror field, a shielded Faraday cup was installed in the longitudinal access port and positioned about 5 cm below the lower mirror peak of the second stage. This insures that the deuteron gyroradius is large in comparison with the dimensions of the cup entrance.

Figure 7 shows the positive ion current into the Faraday cup as a function of time. The waveform shows that the particle loss continues as long as there is first-stage electric field. Oscillations on this waveform have a duration of about 0.4μsec, which corresponds to the ion rotational period around the mean radius of the chamber. The amplitude of the end-loss signal corresponds to a flux of 1.3×10^{14} particles/cmμsec. To measure the distribution function of end-loss particles, an electrostatic energy analyzer[11] was connected to the longitudinal access port. The results are shown in Fig. 8. The error

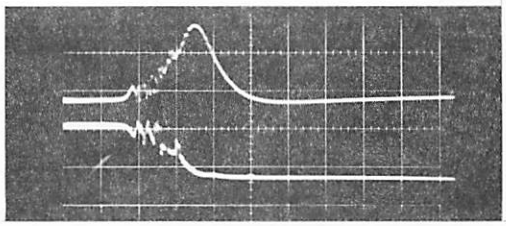

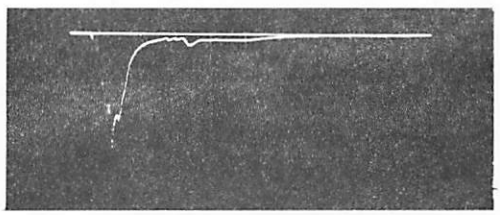

Fig. 7. Waveform of the end loss signal into a shielded Faraday cup. 20 μs/cm.

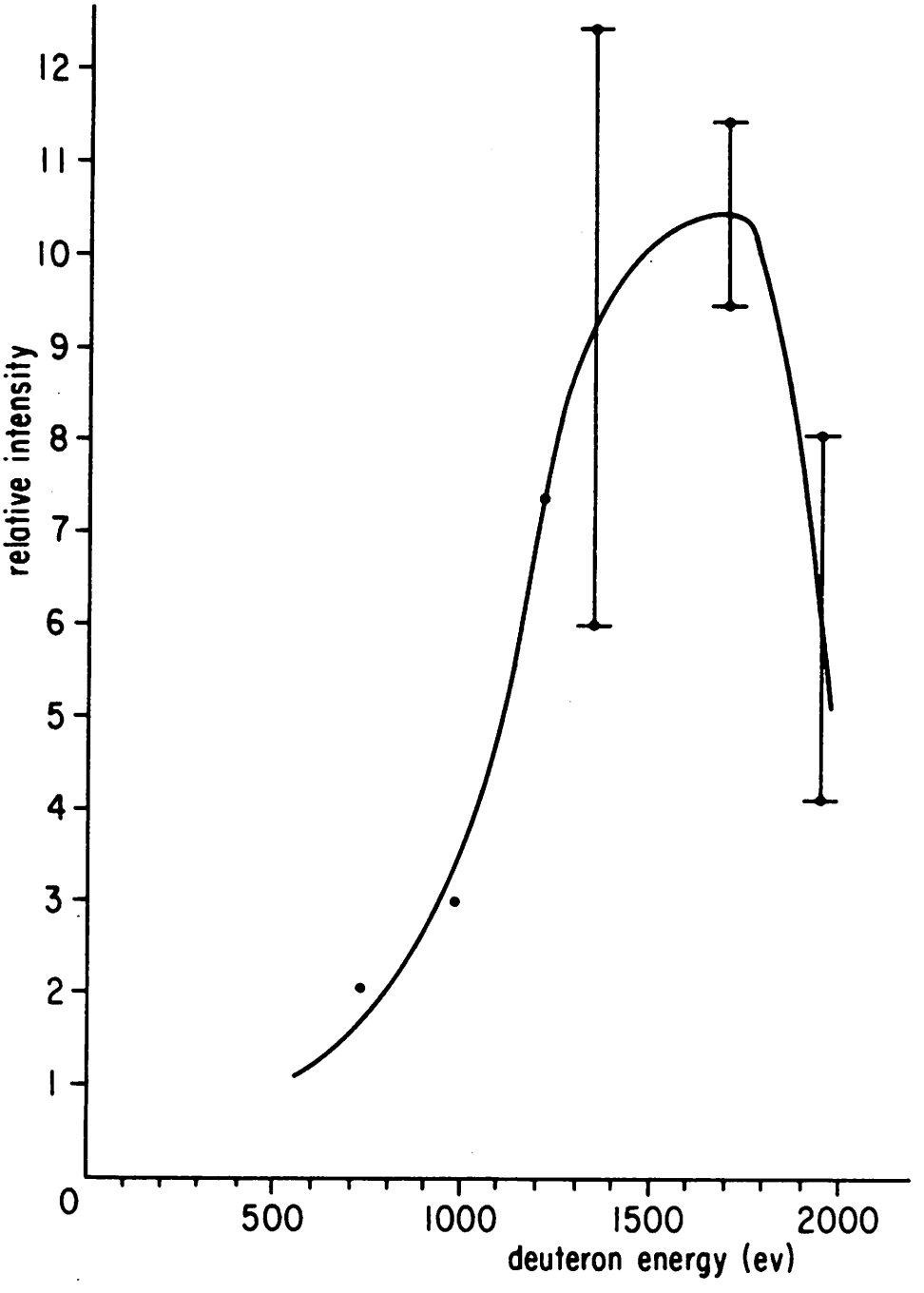

Fig. 8. Plot of the peak signal from the energy analyzer as a function of the energy accepted by the analyzer.

bars represent the extremes of several runs. The most probable energy from these data is 1700 eV, which compares with the calculated value from the estimated electric field. This indicates that it is unlikely that there is significant energy gain from the fringing electric field near the anode tip as the ions leak out of the first stage. Similarly, this shows that as the ions escape there is no significant energy transfer from the bulk rotation or drift motion gyromotion. The loss of this drift energy appears as a reverse torque that results from the shift of the guiding center caused by the polarization drift as the electric field seen by the particle goes to zero during its escape. If the electrode was extended through the second stage so that this orbit shift could not constitute a current, the plasma would continue to rotate as it leaves the field.

To estimate the velocity distribution of the end-loss particles, the second stage mirror field was systematically increased. It was found that by operating this field at 45 kG, the end-loss flux could be reduced to zero. Assuming adiabatic behavior in the region between the first- and second-stage mirror peaks, it can be shown that $W_{\parallel} \doteq \frac{2}{3} W_{\perp}$ at the first-stage mirror peak. There is no external process to produce such a distribution of energy.

In this experiment the avalanche breakdown mechanism creates a rotating plasma that has a particle energy distribution function with a narrow energy spread about some particular perpendicular energy. Such a plasma may be subject to several electrostatic instabilities associated with anisotropic non-Maxwellian distribution functions. Rosenbluth and Post[12] made stability calculations for mirror loss cone

distributions and found from quasi-linear theory that the effect of such an energy distribution is to transfer energy from $W_\perp$ into $W_{||}$. Their distribution function is more Maxwellian than that of a rotating plasma; consequently, their resultant critical length for instability is much longer than the experiment. The stability condition therefore depends critically on the reflection condition.

A second, possible instability mechanism was first proposed by Rosenbluth, Rostoker, and Krall.[13] While their theory would lead to radial flutes, it is possible that an axial loss will also develop. In the presence of a strong electric field it is not difficult for the $\vec{E} \times \vec{B}$ rotation to exceed the rotation associated with diagmagnetic plasma currents--a necessary condition for hydromagnetic instability. Recent work by F. F. Chen[14] expands this theory to show that such rotating plasmas should be highly unstable and lead to electrostatic oscillations at a frequency similar to that observed. This instability mechanism would also depend on the presence of the radical electric field as is observed in Fig. 7. It is not obvious, however, that this instability could provide sufficient $E_{||}$ to cause the observed axial loss.

D. Transfer and Trapping

As originally conceived, this experiment was designed to trap plasma in the first stage and then transfer it to the second stage where it could be heated by additional adiabatic compression. However, as can be seen from the waveform of the diamagnetic pick-up loops in Fig. 2, the plasma does not last long enough to permit the necessary programming of the magnetic field coils to accomplish this transfer.

The other method of combining the features of crossed-field ionization and adiabatic compression is to have a gradient magnetic field in the first stage accelerate the plasma out of the first stage and inject it into the rising mirror-field of the second stage. It has been reported that particle velocities of 2×10^7 cm/sec along the magnetic field have been obtained with this method.[15] Similar results were obtained with this experiment.

If the instability process does not transfer energy from $W_\perp$ to $W_\parallel$ too rapidly, in comparison with the rate in the presence of an axial gradient of the magnetic field, adiabatic trapping in a rising mirror field is possible.

Axial injection into a rising magnetic mirror field requires that the field increase in time as[16]

$$\frac{dB(m)}{dt} \geq B(m)\left(\frac{R}{R-1}\right)^{1/2} \frac{\gamma^2}{2L/v_0} . \tag{6}$$

Here the mirror ratio is denoted by R and is constant in time, L is the distance between mirrors, γ^2 is the ratio of parallel energy $W_\perp(m)$ at the magnetic mirror peak, B(m) is the magnetic induction at the mirror peak, and v_0 is the total velocity. To calculate the peak mirror field required in the second stage at the time of transfer of an arbitrary energy distribution in the upstream field B(x), the mirror equation is used to give

$$\frac{dB(m)}{dt} \geq \left[\frac{R}{R-1}\right]^{1/2}\left[B(x)\left(1 + \frac{W_\parallel(x)}{W_\perp(x)}\right) - B(m)\right]\frac{v_0}{2L} . \tag{7}$$

For slowly rising fields of a few hundred gauss per microsecond, this is satisfied by

$$B(m) \approx B(x)\left[1 + \frac{W_{||}(x)}{W_{\perp}(x)}\right]. \qquad (8)$$

This condition is easily satisfied for rotating plasmas where $W_{\perp}(x) > W_{||}(x)$ except where the particles have acquired a large parallel velocity from $\vec{\mu} \cdot \nabla B$ acceleration or, as is suspected in this case, from some instability mechanism. In the experiments reported here, only a very small fraction of the plasma is trapped as evidenced by the small tail in Fig. 7. This end-loss waveform is essentially the same whether a mirror field or a gradient field was used in the first stage. This indicates that the energy transfer rate is faster from the instability than from $\vec{\mu} \cdot \nabla B$.

E. Electron Temperature and Impurity Radiation

Because of the large initial temperature difference between the ions and electrons, the electrons should be heated very rapidly until the electron temperature is about a hundred volts. This is based on the Spitzer[17] formula which assumes Maxwellian distributions; however, calculations by Kileen et al.[18] predict a slower rate of electron heating for non-Maxwellian distributions. In this experiment, rates of a few hundred electron volts per microsecond are expected for temperatures corresponding to the E/B drift velocity.

To measure the electron temperature in the first stage, the bremsstrahlung radiation was measured through thin foils of Be, Al, and Ni.[19] The results of these measurements indicate an electron

temperature of 500 eV; too large to be bremsstrahlung from electrons. The most likely source of this radiation is the collision of deuterons with the anode as a result of polarization drift. This is consistent with the conclusions obtained from the data of Fig. 6. Similar bremsstrahlung measurements carried out for the second stage were inconclusive in that there was no detectable radiation. This places an upper limit on the second-stage electron temperature of 30 eV. This is confirmed by the ratio of line intensities of C(IV)/C (III) and 0(VI)/0 (V).[19]

A low electron temperature is most likely a consequence of impurity radiation losses in the visible and vacuum ultraviolet range. To measure the impurity spectrum, a quartz prism spectrograph was oriented to receive radiation at the longitudinal access port from the plasma and electrode regions of the first stage. The impurity spectrum shown in Fig. 9 was obtained for the case of no external crowbarring of the discharge. It is included here simply as a reference of strong lines produced when a plasma interacts with a stainless steel system and to demonstrate that rotating plasmas of this type contain a significant amount of impurities from electrode materials.

If a lens system is used to focus the spectrograph on the plasma region and eliminate the electrode light, almost no radiation is observed. This is consistent with the results obtained by using a long exposure time photograph (Fig. 10) of the internal crowbar above the upper mirror coil. The picture was taken through the longitudinal access port with a 10^{-3} neutral density filter and a 300 Å to reduce the light intensity. The radial probe ports in the first stage provide

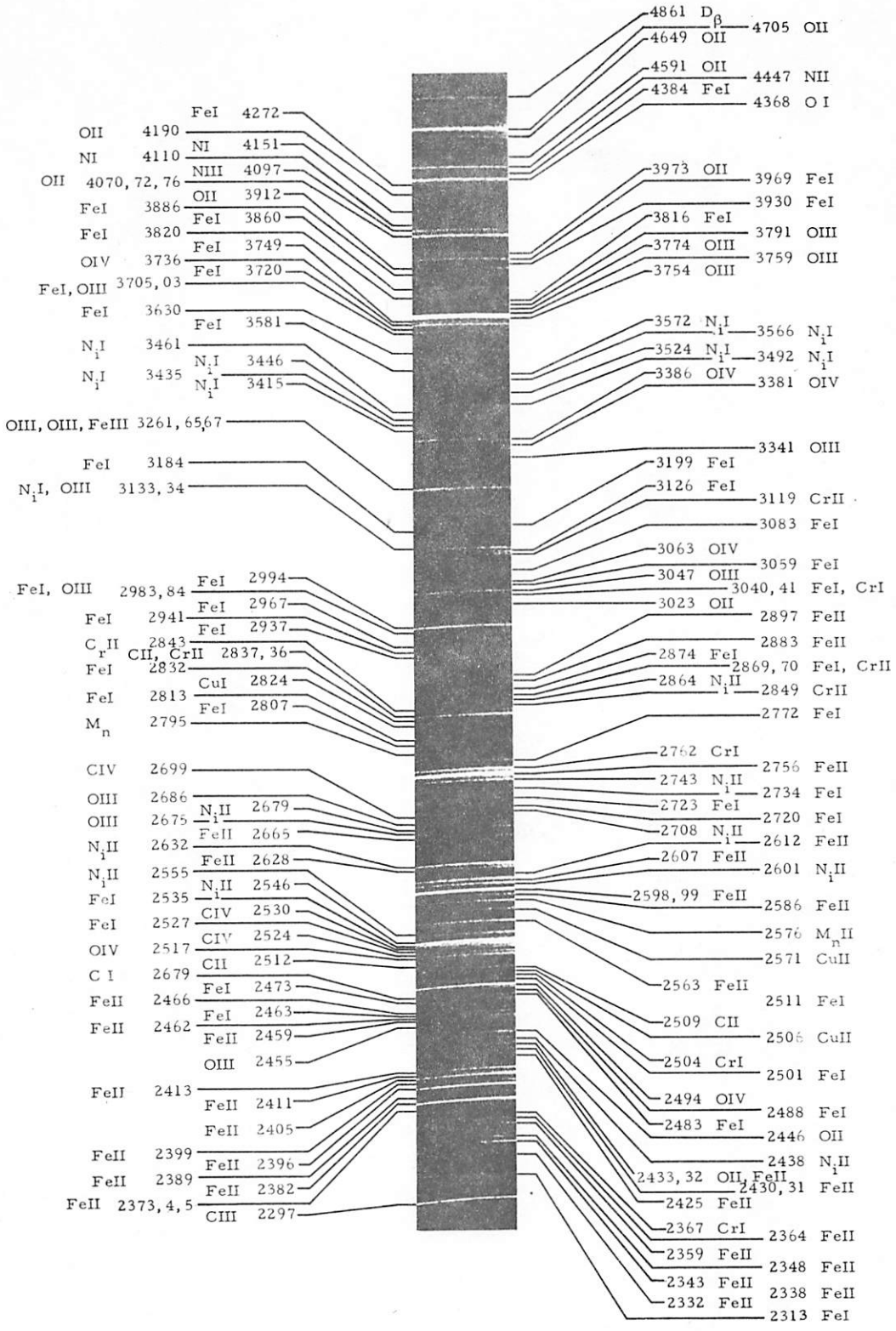

Fig. 9. Expanded view of identified impurity spectrum.

the spatial orientation to conclude that the bright discharge occurs at the upper mirror coil position. The bright ring on the cathode is the point where the field lines which tie the anode and cathode together, intersect the cathode. The dark spot in the center represents the near tip of the anode.

F. Neutron Production

On the basis of the measured first-stage plasma temperature and density, a DD reaction rate of 2×10^8 reactions/cm^3-sec is expected. This corresponds to 3×10^6 neutrons per pulse for a plasma volume of 750 cm^3 and a 20μsec pulse duration. The neutron detector is a L_i^6 scintillator that receives neutrons thermalized in an 8 × 5 cm diameter polyethylene block. The photomultiplier assembly and scintillator are encased with a lead shield 1 cm thick to reduce the possibility of gamma-ray interference. With this method, it is not possible to have a time-resolved history of the neutron production; however, discharges in which the external crowbar immediately followed avalanche breakdown gave the same flux as a discharge in which no external crowbar was applied, that is, about 10^5 - 10^6 neutrons. From previous data, it is known that the plasma lasts an order of magnitude longer without the external crowbar. This suggests that the neutron production occurs very early in the discharge and is a result of deuterons colliding with cold gas on the cathode rather than from plasma reactions. This is consistent with the observation that neutron production is a function of applied voltage. The neutron production was doubled by increasing the cathode anode voltage from 25 to 30 kV, while the value of $\langle \sigma v \rangle$ increased almost an order of magnitude.

Fig. 10. Upstream internal crowbar. Bright ring is located at the upstream mirror peak.

IV. CONCLUSIONS

The formation and the properties of plasma created in the first stage of a combined rotating plasma and magnetic mirror compression experiment, using a fast-pulse gas valve injection method, have been studied. The transfer of plasma from the first stage, where it is formed, to the second or compression stage by adiabatic transfer of a moving mirror and by a gradient injection method were also investigated.

Although the temperature and density of the first-stage plasma favor the use of rotating plasmas as sources for magnetic mirror compression experiments, the polarization drift and fringing field effects caused serious problems that could not be overcome in this configuration. An axial loss mechanism essentially eliminated any possibility of transferring and compressing the plasma in the second stage. This axial loss was investigated and is postulated to be due to the highly anisotropic velocity distribution inherent in rotating plasmas; however, because the rotational velocity is large in comparison with the plasmas diamagnetic rotation, other centrifugal instabilities are possible.

ACKNOWLEDGMENTS

The authors acknowledge with pleasure the many helpful discussions and suggestions made by Drs. Stirling A. Colgate and Klaus Halbach and Messrs. W. R. Baker and K. W. Ehlers during the course of this work.

VI. REFERENCES

1. J. M. Wilcox, Rev. Modern Phys., 31, 1045 (1959).
2. B. A. Tozer, Proc. Inst. Elect. Engrs., 112, 218 (1965).
3. K. Halbach, W. R. Baker, and R. W. Layman, Phys. Fluids, 5, 1482 (1962).
4. H. K. Forsen, Ph.D. thesis, Univ. of Calif., Berkeley (1965), Electronics Research Laboratory Report 65-16.
5. H. K. Forsen, Rev. Sci. Instr., 35, 1362 (1964).
6. O. A. Anderson, W. R. Baker, A. Bratenahl, H. P. Furth, J. Ise, Jr., W. B. Kunkel, and J. M. Stone, Proceedings of the Second United Nations International Conference on the Peaceful Uses of Atomic Energy (United Nations, Geneva, 1958). Vol. 32, 275.
7. K. Halback and W. R. Baker, Phys. Fluids Supp., 7, S62 (1964).
8. D. A. Baker, J. E. Hammel, and F. L. Ribe, Phys. Fluids, 4, 1534 (1961).
9. C. L. Longmire, Elementary Plasma Physics, Interscience (1963), Ch. 4.
10. M. S. Ioffe, R. I. Sobolev, V. G. Tel'Kovskii, and E. E. Yushmanov, Soviet Phys.-JETP, 12, 1117 (1961). (Earlier references to the Ion Magnetron exist in several places and date back as early as 1952).
11. H. P. Eubank and T. D. Wilkerson, Rev. Sci. Instr., 34, 12 (1963).
12. N. M. Rosenbluth and R. F. Post, Phys. Fluids, 8, 547 (1965).

13. N. M. Rosenbluth, N. A. Krall, N. Rostoker, Nuclear Fusion Supp. Pt. 1, 143 (1962).

14. F. F. Chen, "Centrifugal Instabilities," Paper C11S, presented at the 7th Annual Meeting of the APS Plasma Physics Division Nov. 1965, San Francisco. Also, Princeton Physics Laboratory Report MATT 385.

15. K. W. Ehlers, W. R. Baker, and K. Halback, Bull. Am. Phys. Soc., 10, 233 (1965).

16. R. F. Post, Sixteen Lectures on Controlled Thermonuclear Reactions, UCRL 4231.

17. L. Spitzer, Physics of Fully Ionized Gases, Interscience (1956), p. 80.

18. J. Kileen, W. Heckrotte, and G. Boer, Nuclear Fusion Supp., Pt. 1, 183 (1962).

19. F. C. Jahoda, E. M. Little, W. E. Quinn, G. A. Sawyer, and T. F. Stratton, Phys. Rev., 119, 843 (1960).

20. H. R. Griem, Plasma Spectroscopy (McGraw-Hill Book Co., Inc., New York, 1964), pp. 276-278.